Research Article | Vol. 9, No. 6 | 1 Jun 2018 | BIOMEDICAL OPTICS EXPRESS 2671
Biomedical Optics EXPRESS

Advanced easySTED microscopy based on two-photon excitation by electrical modulations of light pulse wavefronts

KOHEI OTOMO,[1,2] TERUMASA HIBI,[1] YI-CHENG FANG,[3] JUI-HUNG HUNG,[3] MOTOSUKE TSUTSUMI,[1] RYOSUKE KAWAKAMI,[1,2] HIROYUKI YOKOYAMA,[3] AND TOMOMI NEMOTO[1,2,*]

[1]*Research Institute for Electronic Science, Hokkaido University, Kita 20 Nishi 10, Kita-ku, Sapporo 001-0020, Japan*
[2]*Graduate School of Information Science and Technology, Hokkaido University, Kita 14 Nishi 9, Kita-ku, Sapporo 060-0814, Japan*
[3]*New Industry Creation Hatchery Center (NICHe), Tohoku University, Aramaki-Aoba 6-6-10, Aoba-ku, Sendai 980-8579, Japan*
**tn@es.hokudai.ac.jp*

Abstract: We developed a compact stimulated emission depletion (STED) two-photon excitation microscopy that utilized electrically controllable components. Transmissive liquid crystal devices inserted directly in front of the objective lens converted the STED light into an optical vortex while leaving the excitation light unaffected. Light pulses of two different colors, 1.06 and 0.64 μm, were generated by laser diode-based light sources, and the delay between the two pulses was flexibly controlled so as to maximize the fluorescence suppression ratio. In our experiments, the spatial resolution of this system was up to three times higher than that obtained without STED light irradiation, and we successfully visualize the fine microtubule network structures in fixed mammalian cells without causing significant photo-damage.

OCIS codes: (180.2520) Fluorescence microscopy; (180.4315) Nonlinear microscopy; (140.5960) Semiconductor lasers; (230.3720) Liquid-crystal devices.

References and links

1. W. Denk, J. H. Strickler, and W. W. Webb, "Two-photon laser scanning fluorescence microscopy," Science **248**(4951), 73–76 (1990).
2. Y. Kusama, Y. Tanushi, M. Yokoyama, R. Kawakami, T. Hibi, Y. Kozawa, T. Nemoto, S. Sato, and H. Yokoyama, "7-ps optical pulse generation from a 1064-nm gain-switched laser diode and its application for two-photon microscopy," Opt. Express **22**(5), 5746–5753 (2014).
3. R. Kawakami, K. Sawada, Y. Kusama, Y.-C. Fang, S. Kanazawa, Y. Kozawa, S. Sato, H. Yokoyama, and T. Nemoto, "In vivo two-photon imaging of mouse hippocampal neurons in dentate gyrus using a light source based on a high-peak power gain-switched laser diode," Biomed. Opt. Express **6**(3), 891–901 (2015).
4. S. W. Hell, "Far-field optical nanoscopy," Science **316**(5828), 1153–1158 (2007).
5. B. Huang, H. Babcock, and X. Zhuang, "Breaking the diffraction barrier: super-resolution imaging of cells," Cell **143**(7), 1047–1058 (2010).
6. S. W. Hell and J. Wichmann, "Breaking the diffraction resolution limit by stimulated emission: stimulated-emission-depletion fluorescence microscopy," Opt. Lett. **19**(11), 780–782 (1994).
7. T. A. Klar, S. Jakobs, M. Dyba, A. Egner, and S. W. Hell, "Fluorescence microscopy with diffraction resolution barrier broken by stimulated emission," Proc. Natl. Acad. Sci. U.S.A. **97**(15), 8206–8210 (2000).
8. G. Moneron and S. W. Hell, "Two-photon excitation STED microscopy," Opt. Express **17**(17), 14567–14573 (2009).
9. K. T. Takasaki, J. B. Ding, and B. L. Sabatini, "Live-cell superresolution imaging by pulsed STED two-photon excitation microscopy," Biophys. J. **104**(4), 770–777 (2013).
10. P. Bethge, R. Chéreau, E. Avignone, G. Marsicano, and U. V. Nägerl, "Two-photon excitation STED microscopy in two colors in acute brain slices," Biophys. J. **104**(4), 778–785 (2013).
11. M. Reuss, J. Engelhardt, and S. W. Hell, "Birefringent device converts a standard scanning microscope into a STED microscope that also maps molecular orientation," Opt. Express **18**(2), 1049–1058 (2010).

#318596 https://doi.org/10.1364/BOE.9.002671
Journal © 2018 Received 28 Dec 2017; revised 22 Mar 2018; accepted 6 Apr 2018; published 15 May 2018

Biomedical Optics EXPRESS

12. F. Görlitz, P. Hoyer, H. J. Falk, L. Kastrup, J. Engelhardt, and S. W. Hell, "A STED microscope designed for routine biomedical applications," Prog. Electromagnetics Res. **147**, 57–68 (2014).
13. K. Otomo, T. Hibi, Y. Kozawa, M. Kurihara, N. Hashimoto, H. Yokoyama, S. Sato, and T. Nemoto, "Two-photon excitation STED microscopy by utilizing transmissive liquid crystal devices," Opt. Express **22**(23), 28215–28221 (2014).
14. S. Ipponjima, T. Hibi, Y. Kozawa, H. Horanai, H. Yokoyama, S. Sato, and T. Nemoto, "Improvement of lateral resolution and extension of depth of field in two-photon microscopy by a higher-order radially polarized beam," Microscopy (Oxf.) **63**(1), 23–32 (2014).
15. N. Hashimoto and M. Kurihara, "Liquid crystal quantized GRIN lens and its application to AF systems," Proc. SPIE **7232**, 808123 (2009).
16. A. K. Dutta, K. Kamada, and K. Ohta, "Spectroscopic studies of nile red in organic solvents and polymers," J. Photochem. Photobiol. Chem. **93**(1), 57–64 (1996).
17. M. Booth, D. Andrade, D. Burke, B. Patton, and M. Zurauskas, "Aberrations and adaptive optics in super-resolution microscopy," Microscopy (Oxf.) **64**(4), 251–261 (2015).
18. T. J. Gould, D. Burke, J. Bewersdorf, and M. J. Booth, "Adaptive optics enables 3D STED microscopy in aberrating specimens," Opt. Express **20**(19), 20998–21009 (2012).
19. A. Tanabe, T. Hibi, S. Ipponjima, K. Matsumoto, M. Yokoyama, M. Kurihara, N. Hashimoto, and T. Nemoto, "Correcting spherical aberrations in a biospecimen using a transmissive liquid crystal device in two-photon excitation laser scanning microscopy," J. Biomed. Opt. **20**(10), 101204 (2015).
20. A. Tanabe, T. Hibi, S. Ipponjima, K. Matsumoto, M. Yokoyama, M. Kurihara, N. Hashimoto, and T. Nemoto, "Transmissive Liquid-crystal device for correcting primary coma aberration and astigmatism in biospecimen in two-photon excitation laser scanning microscopy," J. Biomed. Opt. **21**(12), 121503 (2016).
21. M. Leutenegger, C. Eggeling, and S. W. Hell, "Analytical description of STED microscopy performance," Opt. Express **18**(25), 26417–26429 (2010).
22. S. Schrof, T. Staudt, E. Rittweger, N. Wittenmayer, T. Dresbach, J. Engelhardt, and S. W. Hell, "STED nanoscopy with mass-produced laser diodes," Opt. Express **19**(9), 8066–8072 (2011).
23. J.-H. Hung, K. Sato, Y.-C. Fang, L.-T. Peng, T. Nemoto, and H. Yokoyama, "Generation of high-peak-power sub-nanosecond 650-nm band optical pulses based on semiconductor laser controlling technologies," Appl. Phys. Express **10**(10), 102701 (2017).
24. G. Vicidomini, G. Moneron, K. Y. Han, V. Westphal, H. Ta, M. Reuss, J. Engelhardt, C. Eggeling, and S. W. Hell, "Sharper low-power STED nanoscopy by time gating," Nat. Methods **8**(7), 571–573 (2011).
25. I. C. Hernández, M. Castello, L. Lanzanò, M. d'Amora, P. Bianchini, A. Diaspro, and G. Vicidomini, "Two-Photon Excitation STED Microscopy with Time-Gated Detection," Sci. Rep. **6**(1), 19419 (2016).

1. Introduction

Two-photon excitation laser scanning microscopy (TPLSM) is a powerful tool for visualizing microstructures in living specimens [1]. Since the two-photon excitation probability is proportional to the square of the excitation light power, the excitations are spatially localized at the focus of the objective lens, allowing optically-sectioned fluorescent images to be obtained. Most of the fluorophores used in TPLSM can be excited by a near-infrared (NIR) light pulse, which has the advantages of superior penetration depth and reduced invasiveness for biological specimens. We have previously improved the penetration depth further by developing a gain-switched semiconductor laser diode (GSLD)-based light source [2] that enabled us to successfully visualize hippocampal neurons in the dentate gyrus of an anesthetized mouse brain 1.6 mm below the surface [3]. Our success was mainly attributed to the higher peak power and longer temporal stability of this GSLD-based light source relative to the mode-locked titanium–sapphire (Ti–Sa) laser light sources that were conventionally used in TPLSM systems: its repetition rate and pulse timing were electrically controlled and highly stable [2].

Over the past decade, several super-resolution microscopy techniques have been proposed that can overcome diffraction limitations [4, 5]. One such technique, stimulated emission depletion (STED) microscopy, was described theoretically in 1994 [6], and was used to actually visualize biological nanostructures [7]. STED microscopy utilizes a high-power donut-shaped light (STED light) to induce stimulated emission and restrict the spontaneous emission area to below the diffraction limit. The excitation and STED lights should be superimposed spatially, and also temporally when pulsed lasers are used. The spatial resolution of TPLSM was improved by applying the STED technique [8], and the resulting STED two-photon excitation (STED-TP) microscopy procedure was used to visualize the

Biomedical Optics EXPRESS

nanostructures of dendritic spinal necks in acute brain slices, 50–100 μm below their surfaces [9, 10].

In general, both STED and STED-TP microscopy require a large-scale optical setup, since these systems generally require separate optical paths for the excitation and STED lights. In addition, optical elements are required to spatially modulate the STED light and/or control the timing of the individual excitation and STED light pulses, making the whole system quite large. To build a more compact STED microscopy system, unique segmented wave plates have been employed to create a single optical path, only modulating the STED light and leaving the excitation light unaffected [11]. In recent years, systems where the excitation and STED lights pass through a common beam-shaping device have been implemented commercially, and this is known as easySTED microscopy [12]. Our group has also developed a simplified STED-TP microscopy system that utilizes transmissive liquid crystal (LC) devices (tLCDs) to create an optical vortex for use with the STED light [13]. These tLCDs, which are only placed in the optical path, can be electrically controlled to act as spatial light modulators (SLMs) that modify the transmitted light's optical properties, such as its phase, polarization, and laser light intensity, with high conversion efficiency. Furthermore, tLCDs can be applied over a wide wavelength region simply by changing the applied voltage [13, 14]. Since tLCDs are compact, we also realized that they could be inserted between the objective lens and the microscope revolver [14].

In this paper, we developed a novel STED-TP microscopy system where the excitation and the STED light pulses generated by using compact electrically-modulated laser diode (LD)-based light sources. tLCDs were inserted directly in front of the objective lens and only modulated the STED light, meaning that our tLCD-based STED-TP microscopy system was conceptually similar to easySTED microscopy [11, 12]. Moreover, by controlling the voltages applied to the tLCDs, our system can employ several other wavelengths of STED light, unlike easySTED. We therefore called our approach advanced easySTED-TP microscopy. Using this system, we successfully visualized tiny fluorescent dye-labeled beads and microtubule network structures in fixed mammalian cells with superior spatial resolution and without causing significant photo-damage.

2. Materials and methods

2.1 Optical setup

Figure 1 shows an overview of our laser light sources. For two-photon excitation, we used a GSLD-based light source that was produced in-house [2], consisting of an electrical pulse generator, an NIR distributed feedback laser diode (DFB-LD), and an optical fiber amplifier chain. This operated at a repetition rate of 10 MHz using external trigger signals from a timing controller (T560; Highland Technology). The basic configuration of the optical fiber chain, of which components were coupled with optical fiber, was as given in our previous report [3], except for the main amplifier. In this study, we utilized a large-core ytterbium-doped fiber amplifier (made in-house) as the main amplifier, obtaining an average output power of approximately 1 W. The red laser light pulses used for STED were generated using a can-type LD (GH0641FA2C; Sharp Corp.) with an electrical pulse generator (T165; Highland Technology) that operated at a repetition rate of 10 MHz using external trigger signals from the other channel of the timing controller. The STED light was coupled into a single-mode fiber for spatial-mode cleaning. The powers of the two-photon excitation and the STED light pulses were adjusted respectively by using two sets of a half-wave plate and a Glan-laser polarizer. Next, the two differently-colored light beams were collimated and introduced into the advanced easySTED-TP microscopy system, described below.

Figure 2(a) shows a schematic of our new microscopy system. The linearly-polarized two-photon excitation light beam and the orthogonal linearly-polarized STED light beam by passing through a half-wave plate were joined into a single optical path at a first dichroic mirror (RDM800; Olympus Corp.) and introduced into a galvano-mirror scanner (C2; Nikon

Biomedical Optics EXPRESS

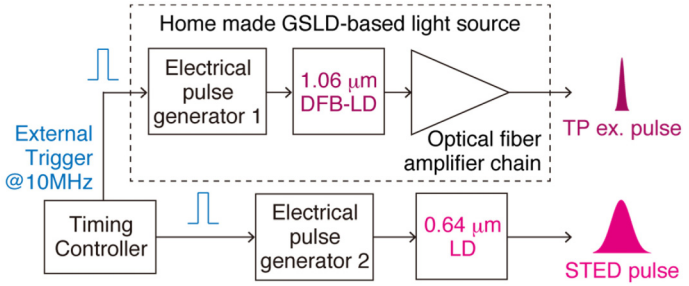

Fig. 1. Overview of the two-photon excitation (TP ex.) and STED light sources. DFB: distributed feedback; GS: gain-switched semiconductor; LD: laser diode.

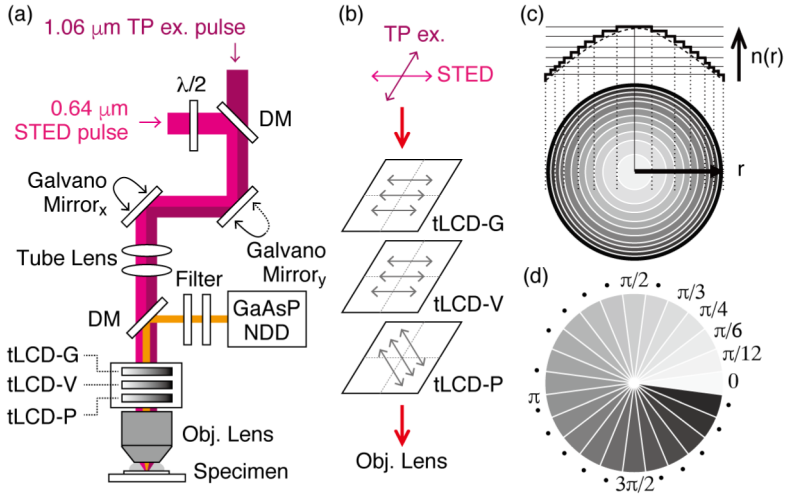

Fig. 2. (a) Schematic of our advanced easySTED-TP microscopy system. DM: dichroic mirror; GaAsP NDD: gallium arsenide phosphide-based non-descanned detector; GSLD: gain-switched laser diode; tLCD-G: transmissive liquid crystal device-based gradient index lens; tLCD-P; plain cell tLCD; tLCD-V: tLCD used to create optical vortices; λ/2: half-wave plate. (b) Polarization directions of the TP ex. and STED light beams and orientations of LC molecules in three different types of tLCDs. (c) Concentric transparent electrode pattern and phase distribution profile for a tLCD-G. (d) Theoretical phase distribution of the optical vortex generated by a tLCD-V.

Corp.) equipped with an upright microscope (ECLIPSE FN1; Nikon Corp.) These two differently-colored light beams were introduced into three different types of tLCDs, those were placed between the objective lens and the revolver [14]. Figure 2(b) shows polarization directions of the two differently-colored light beams and orientations of LC molecules in three different types of tLCDs. When the polarization of transmitting light beams coincided with the orientation of LC molecules, optical retardations of light beams could be modulated. The first tLCD was a 24-zone divided tLCD based gradient index (GRIN) lens (tLCD-G) formed with a concentric transparent electrode pattern (Fig. 2(c)). tLCD-G modulated only the convergence angle of the STED light beam and did not affect the two-photon excitation light beam. In the quantized GRIN structure of tLCD-G, the distribution of refractive index was designed as $n(r) = n_0 - r^2/2fd$ where "n_0" was the refractive index at the optical axis, "f" was the focal length, and "d" was the optical guide length (for more details, see Reference [15]). The second tLCD was one that created optical vortices (tLCD-V) (Fig. 2(d)) [13]. tLCD-V converted only the STED light beam to an optical vortex and did not affect the two-photon excitation light beam. The third one was a plain cell tLCD (tLCD-P) consisting of homogeneously-aligned LC molecules that functioned as an applied voltage-dependent

Biomedical Optics EXPRESS

variable wave plate [13]. The LC molecules in the tLCD-P were oriented at an angle of 45° with respect to the linear polarization direction of the STED light beam, converting it to be circularly polarized [13]. The tLCD-P also caused the orthogonal linearly-polarized excitation light beam passing through it to become elliptically polarized. Immediately after the tLCDs, a water immersion objective lens with a numerical aperture of 1.27 (CFI Plan Apo IR 60XWI; Nikon) was used to focus the two differently-colored light pulses onto the specimen. The fluorescent light was first collected by the objective lens and then separated by a second dichroic mirror (T620lpxrxt (0.62 μm long-pass dichroic mirror); Chroma Technology Corp.) To suppress the background signals, leakage of STED light pulses of 0.64 μm to the fluorescent signals were completely removed by two emission filters (BSP01-633R (0.62 μm short-pass filter), FF01-562/40 (0.54 – 0.58 μm band-pass filter); Semrock, Inc.). Thus, the fluorescent light (0.54 – 0.58 μm) was detected by a fluorescent light detector, gallium arsenide phosphide-based non-descanned detector (GaAsP NDD).

The optical properties of the two-photon excitation light pulses were already known from a previous report [2] (central wavelength = 1.06 μm, pulse width = 7.5 ps). To confirm the optical properties of the STED light pulses, a movable sampling reflector was placed in the optical path, in front of the scanner. After moving the reflector into the optical path, light pulses were introduced and analyzed by a spectrum analyzer (AQ-6315A; Yokogawa Electric Corp.) and a sampling oscilloscope (TDS8200, 80E04; Tektronix) with a high-speed photo-detector (1414-50; Newport corp.) Figs. 3(a) and (b) depict the STED light's spectrum and pulse shape, respectively. The spectrum showed two peaks at around 0.64 μm within a range of 0.01 μm, and the pulse shape showed an initial sharp peak, with a width of ca. 0.3 ns and an intensity that is twice that of the pulse components over the subsequent ca. 3 ns.

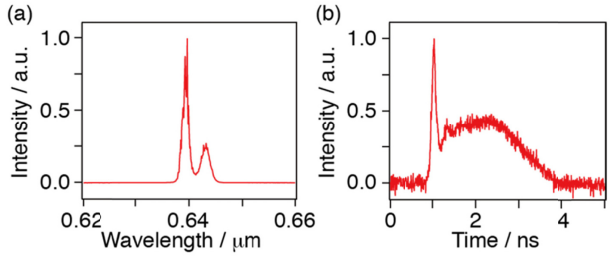

Fig. 3. Optical properties of the STED light pulse. (a) Optical spectrum. (b) Optical pulse shape.

2.2 Sample preparation

Three types of fluorescently-labeled beads (Nile Red, ~1 μm diameter; Nile Red, ~20 nm diameter; and Red, ~100 nm diameter; Thermo Fisher Scientific) were diluted in water (1:3000, v/v), applied dropwise to glass coverslips, and allowed to dry. The coverslips were then mounted using a mounting medium.

Next, HeLa cells were cultured on glass coverslips in Dulbecco's modified Eagle's medium (DMEM; Wako Pure Chemical, Co.), supplemented with 10% fetal bovine serum and penicillin/streptomycin (Thermo Fisher Scientific), at 37°C in a humidified atmosphere containing 5% CO2. The cells were then stained with an anti-α-tubulin antibody (clone DM1A; Cell Signaling Technology) and an ATTO 532-conjugated anti-mouse IgG antibody (Rockland Immunochemicals, Inc.), and mounted using ProLong diamond reagent (Thermo Fisher Scientific).

2.3 Image acquisition and data analysis

The fluorescent images of the 1 μm Nile Red beads and the 100 nm Red beads had a pixel size of 41 nm and a pixel dwell time of 1.9 μs. The fluorescent signals from the 1 μm Nile

Biomedical Optics EXPRESS

Red beads were evaluated by integrating the pixel values after subtracting the background signal. We acquired 10-μm-thick z-stacks at 0.25 μm intervals and used them to reconstruct images of the 100 nm Red beads. The fluorescent images of the 20 nm Nile Red beads had a pixel size of 14 nm and a pixel dwell time of 10.3 μs, and were constructed by averaging the 16 acquired images. The full width at half maximum (FWHM) values were evaluated by fitting their fluorescence intensity profiles around the central intensity using Gaussian functions.

The reconstructed TPLSM images of ATTO532-labelled microtubules had a pixel size of 41 nm and a pixel dwell time of 10.3 μs, and we acquired 10-μm-thick z-stacks at 0.25 μm intervals. When comparing the TPLSM and advanced easySTED-TP images, both images had a pixel size of 21 nm and a pixel dwell time of 10.3 μs, and were constructed by averaging 8 acquired images.

3. Results

First, we confirmed the spatial modulation of the STED light by the tLCDs. As in our previously-reported STED-TP system [13], a tLCD-V and a tLCD-P were used to convert a linearly-polarized Gaussian beam to a circularly-polarized optical vortex. We confirmed the presence of a hollow focal pattern by using the STED light to produce single-photon excitation and record fluorescent images of a 100 nm Red bead (Fig. 4(a)). We also installed a tLCD-G to cancel out the axial focal mismatch between the two-photon excitation and STED lights, which was a consequence of chromatic aberration in the objective lens. This tLCD-G allowed us to modulate the axial focal position of the STED light to within a depth of 0.5 μm by tuning the applied voltage (Fig. 4(b)), and applying the maximum voltage enabled us to successfully match the axial focal positions of the STED and two-photon excitation lights, which were mostly unaffected by the tLCDs (Fig. 4(c)).

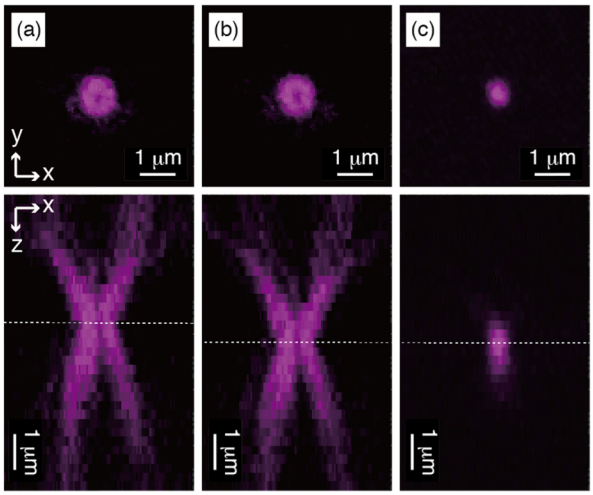

Fig. 4. Reconstructed fluorescent images of a 100 nm Red bead, excited by both the STED and two-photon excitation lights. (a) STED light, minimum voltage applied to the tLCD-G. (b) STED light, maximum voltage applied to the tLCD-G. (c) Two-photon excitation light.

We also recorded two-photon excitation fluorescent images of a 1 μm Nile Red bead to confirm the dependence of the fluorescence suppression ratio on the timing of the two-photon excitation and STED light pulses. In this case, the STED light was not converted to an optical vortex but instead made to produce a Gaussian focal pattern to induce stimulated emission in

Biomedical Optics EXPRESS

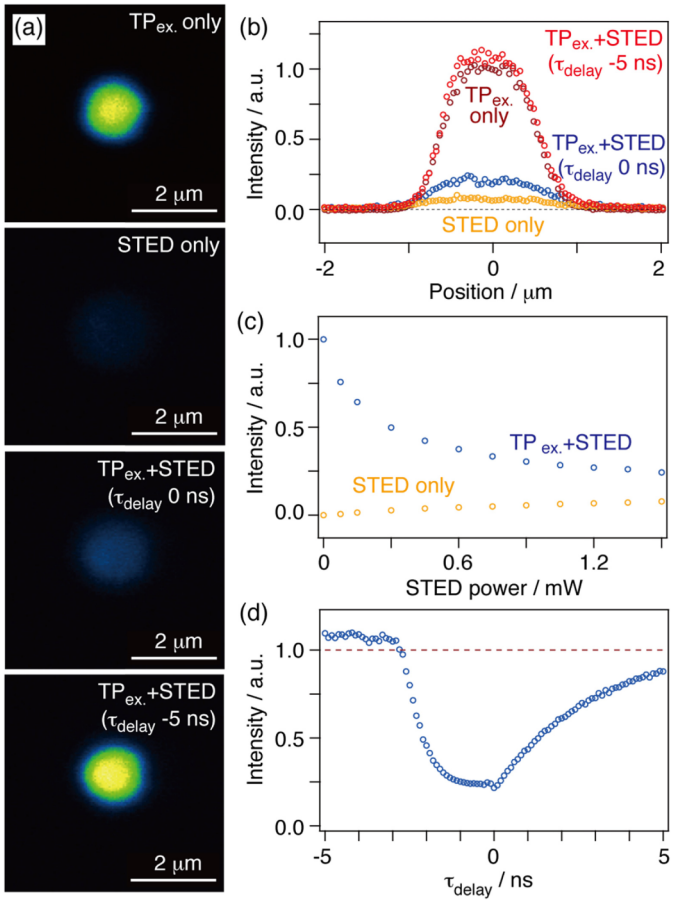

Fig. 5. (a) Fluorescent images of a 1 μm Nile Red bead under four different laser irradiation conditions. (b) Fluorescence intensity profiles around the intensity center and along the *x*-axis of (a). (c) Dependence of fluorescence intensity on STED power for a 1 μm Nile Red bead with and without two-photon excitation. (d) Dependence of the fluorescence intensity of a 1 μm Nile Red bead on the STED light pulse delay time (τ_{delay}). The red dashed line indicates the fluorescence intensity obtained with only NIR light irradiation.

the fluorophores. We used a timing controller to change the relative delay (τ_{delay}) between the STED and two-photon excitation light pulses. Figures 5(a) and (b) show fluorescent images and intensity profiles for a single bead under four different laser irradiation conditions: two-photon excitation light pulses only; STED light pulses only; both types of light pulse, with the timing adjusted so as to maximize the fluorescence suppression ratio (defined as $\tau_{delay} = 0$ ns); and both types of light pulse, with the timings separated by an interval longer than the pulse width and fluorescence lifetime of the fluorophores (e.g., $\tau_{delay} = -5$ ns). The average laser powers of the two-photon excitation and STED lights at the specimen position were 4.0 mW and 1.5 mW, respectively. When τ_{delay} was 0 ns, the fluorescence suppression ratio was approximately 80%, but when τ_{delay} was −5 ns, the fluorescence intensity was slightly higher than for irradiation by NIR light only, possibly because of direct single-photon excitation fluorescence caused by the STED light pulses. Figure 5(c) presents the dependence of the fluorescence intensity on the average STED light power, showing that the fluorescence suppression ratio reached 80% at maximum power (1.5 mW at the specimen position). Under these STED light irradiation conditions, stimulated emission of the fluorophores was not

Biomedical Optics EXPRESS

completely saturated. In addition, the contribution of direct excitation by the STED light to the fluorescence (ca. 8% at maximum power) is plotted on the same graph.

Next, we investigated the effect of changing the timings of the two differently-colored light pulses. Here, τ_{delay} was changed from −5 to 5 ns (in steps of 0.1 ns), and the resulting fluorescence suppression ratios are shown in Fig. 5(d). Between −5 ns and ca. −3 ns, the fluorescence intensity was slightly higher than for irradiation by NIR light only, because the STED light pulse also excited the fluorophores. Between ca. −3 ns and 0 ns, the fluorescence suppression ratio increased sharply due to the temporal overlap between the two types of light pulse. Between 0 ns and 5 ns, the suppression ratio decreased again, as the two types of light pulse became temporally separated. In this region, the fluorophores excited by the previous two-photon excitation pulse were then irradiated by the delayed STED light pulse. This gentle rise in the fluorescence intensity curve must therefore reflect spontaneous emission by the Nile Red fluorophores, for which the fluorescence lifetime in hydrophilic solvents is around 3.5 ns [16].

After optimizing the timings of two differently-colored light pulses, we superimposed the donut-shaped STED light over the two-photon excitation light to evaluate the lateral spatial resolution. The sizes of fluorescent images of targets smaller than the diffraction limit correspond to the lateral spatial resolution, so we recorded an advanced easySTED-TP image of 20 nm Nile Red beads and fitted the resulting values with Gaussian functions to evaluate their fluorescence intensity profiles (Fig. 6). The two-photon excitation light's polarization properties generally cause the lateral focal spot to become elongated along the polarized direction, and we observed larger FWHM values for the *y*-axis than for the *x*-axis. After applying the STED light, the fluorescent beads images decreased in size relative to those obtained without the STED light. Using average laser powers of 3.2 mW and 1.5 mW at the specimen position for the two-photon excitation and STED lights, respectively, the FWHM values obtained along the *x*- and *y*-axes were reduced by 67% (from 413 to 137 nm) and 69% (from 489 to 151 nm), respectively. In other words, the spatial resolution achieved by our new microscopy system was approximately three times higher than that of TPLSM.

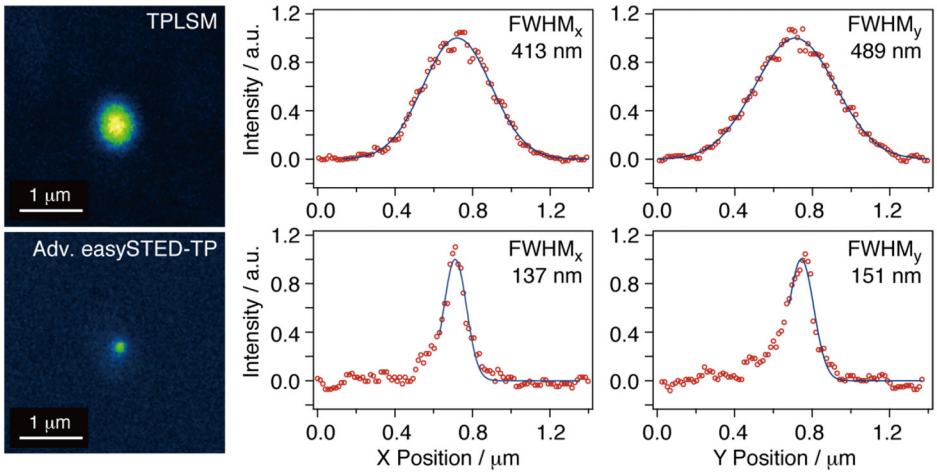

Fig. 6. Comparison of TPLSM and advanced easySTED-TP images of 20 nm Nile Red beads. The upper panels show fluorescent images, while center and lower panels depict the fluorescence intensities around the intensity centers along the *x*- and *y*-axes for the corresponding upper-hand image. The red circles and blue lines indicate the measured values and fitted curves, respectively. The inset length values indicate the FWHM values.

Finally, we observed microtubules in a fixed HeLa cell that had been immunostained with fluorescent dye-labeled antibodies. We selected an ATTO 532 dye because it had the highest fluorescence suppression ratio among other dyes with similar spectral properties. The two-

Biomedical Optics EXPRESS

photon excitation light power at the specimen was 4.0 mW for both imaging procedures, and the STED light power was 1.5 mW. Figure 7 shows that our advanced easySTED-TP microscopy system was able to visualize the microtubule network structures more clearly than TPLSM could. Although the STED light irradiation induced a small amount of photo-bleaching (ca. 10% after recording these images), the photo-bleached regions were restricted to the foci. Thus good images were obtained of the microtubules both just under the coverslip (z = 1.5 μm) and on the opposite side of the same cell (z = 9.0 μm), confirming the effectiveness of our new microscopy system for biological specimens.

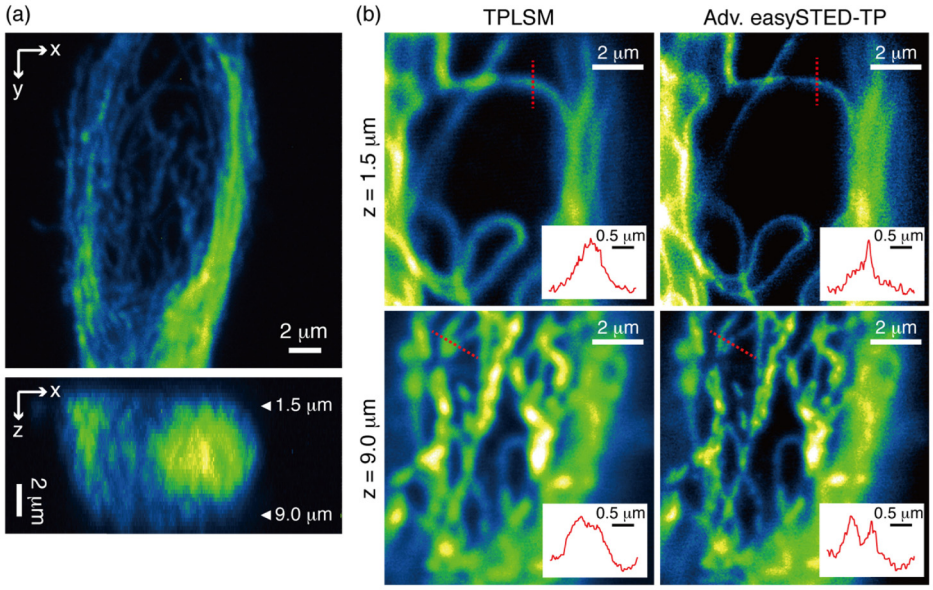

Fig. 7. (a) TPLSM image of microtubule networks in a fixed HeLa cell after immunostaining with ATTO 532-conjugated antibodies, reconstructed from z-stacks. (b) Comparison of TPLSM and advanced easySTED-TP images of basal (1.5 μm below the coverslip) and apical (9.0 μm below the coverslip) regions of (a). The inset panels indicate the fluorescence intensity profiles along the red dashed lines in the fluorescent images.

4. Discussions

Optical properties of specimens such as their spatial refractive index distributions usually cause several optical aberrations to degrade the performance of super-resolution microscopy, including the spatial resolution and fluorescence intensity [17]. SLMs have been used in single-photon excitation STED microscopy to cancel out these optical aberrations [18]. We have recently developed other types of tLCDs for TPLSM with the aim of correcting spherical aberrations [19], primary coma aberrations and astigmatism [20]. These tLCDs would be also useful for our advanced easySTED-TP microscopy system, especially for the regions deep inside thick biological specimens. In addition, the spatial resolution could in principle be improved by increasing the power of the STED light in pulsed STED microscopy [21].

Unfortunately, the maximum peak power of the compact STED light source used in this study, a mass-produced LD, was limited to several hundred mW in pulsed mode, as reported for LD-based single-photon excitation STED microscopy [22]. To improve the spatial resolution, we have thus developed a compact STED light source with a higher peak power that utilizes novel semiconductor laser-control technologies [23].

In this study, we did not utilize concurrent confocal detection, time-gated detection, or deconvolution algorithms, despite the fact that several researchers have suggested these could improve spatial resolution in STED and STED-TP microscopy [24, 25]. Such utilizations

Biomedical Optics EXPRESS

might be expected to further improve the spatial resolution in our advanced easySTED-TP microscopy system, even when using low-power STED lights.

For thick living specimens, several researchers had previously proposed using a pulsed STED-TP microscopy system where Ti–Sa lasers and/or optical parametric oscillators were used for the two-photon excitation or STED lights [10, 11], inevitably resulting in a large-scale optical setup. A simplified optical setup based on sophisticated optical technologies might allow for more stable and easy-to-use observations with STED-TP microscopy, compared with previous complicated pulsed STED-TP microscopy systems.

5. Summary

In this paper, we developed the advanced easySTED-TP microscopy system, which utilized compact, electrically-controllable components, including tLCDs and two types of LD-based light sources. This allowed us to both simplify the whole system and make it more compact, as well as offer long-term observation stability. By optimizing the spatial modulations and controlling the two-photon excitation and STED lights temporally, we were able to improve the spatial resolution by a factor of approximately three compared with TPLSM, for the most suitable fluorescent dye screened (Fig. 6). The STED light power required to achieve the highest spatial resolution was, on average, only 1.5 mW at the specimen, and notably, this did not induce significant photo-bleaching during the observation (Fig. 7). We hope that the fundamental technologies developed here for advanced easySTED-TP microscopy will facilitate visualization of intravital nanostructures, and as well as promote its widespread use in the wider life sciences field and related areas.

Funding

MEXT/JSPS KAKENHI (JP16K15103, JP15H05953 “Resonance Bio”, and JP16H06280 “Advanced Bioimaging Support”); the Research Program of “Five-star Alliance” in “NJRC Mater. & Dev.” (MEXT); and Brain/MINDS, AMED, Japan.

Acknowledgments

We thank Dr. N. Hashimoto, Mr. M. Kurihara and Dr. A. Tanabe of Citizen Watch Co., Ltd. for kindly providing the tLCDs; and Dr. S. Sato and Dr. Y. Kozawa of Institute of Multidisciplinary Research for Advanced Materials, Tohoku University for their helpful advice regarding optical setup; and Dr. K. Kobayashi and Dr. Y. Matsuo of the Nikon Imaging Center at Hokkaido University for providing technical support. We are also grateful for the advice provided by Dr. K. Iijima, Dr. H. Ishii, and Dr. L. Qiao of the Laboratory of Molecular and Cellular Biophysics at the Research Institute for Electronic Science, Hokkaido University.

Disclosures

The authors declare that there are no conflicts of interest related to this article.